Astron. Astrophys. 321, 859–866 (1997)

ASTRONOMY
AND
ASTROPHYSICS

Infrared stellar absorption lines around 1.6 μm: a new metallicity scale for old stellar populations⋆

L. Origlia[1], **F.R. Ferraro**[2], **F. Fusi Pecci**[2], **and E. Oliva**[3]

[1] Osservatorio Astronomico di Torino Strada Osservatorio 20, I-10125 Pino Torinese, Italy
[2] Osservatorio Astronomico di Bologna Via Zamboni 33, I-40126 Bologna, Italy
[3] Osservatorio Astrofisico di Arcetri, Largo E.Fermi 5, I-50125 Firenze, Italy

Received 4 June 1996 / Accepted 5 November 1996

Abstract. A new metallicity scale (accurate to within $\pm$0.3 dex) for old stellar systems is derived and discussed. It is particularly useful in cool objects with [Fe/H]$\gtrsim$–1.3 and is based on medium resolution ($R \sim 2000$) near infrared spectra of a deep and relatively isolated feature at 1.62 μm which is mostly due to the CO(6,3) second overtone band–head. The value of [Fe/H] can be determined using handy interpolation formulae (Eqs. 1a, 1b and Eq. 2) and is little influenced by anomalies of the carbon abundance, [C/Fe], since the growth of W_λ(1.62) with metallicity primarily tracks variations of stellar temperature and gravity, rather than the increase of the total carbon abundance.

The method is tested using IRSPEC observations of 13 well known globular clusters where the derived [Fe/H] values are in good agreement with the results of Zinn (1985) for all but two objects, namely NGC6624 and Terzan 5, which we find much less ($\simeq$0.9 dex) metallic (first two columns of Table 1 and Fig. 5). Ellipticals are found to have [Fe/H]$\simeq$–0.4 and $\sim$0.5 dex below estimates based on the Mg_2 index, this indicates that Mg may be overabundant by a similar amount. A $\sim$0.5 dex enhancement of Si (another α element) is also suggested by the strength of the 1.59 μm line in our spectra. The only object with [Fe/H]$\gtrsim$0.0 is the globular cluster Terzan 1.

Key words: stars: late type – stars: population II – globular clusters: general – infrared: stars – stars: abundances

1. Introduction

The definition of a metallicity scale for distant stellar clusters and galaxies requires a proper set of integrated indices which trace the average properties of the dominant stellar population, and which should be calibrated on well studied stellar clusters. In this paper we analyze the IR spectroscopic properties of a representative sample of Galactic globular clusters (GGCs) both in the halo and in the disk as a function of the cluster metallicity [Fe/H] to obtain suitable indicators of the metal content in old stellar populations. The location of the red giant branch (RGB) in the HR diagram of GGCs, i.e. the average temperature of the coolest stellar component which dominates their IR luminosity, is directly related to the cluster metal content, the higher [Fe/H] the cooler the stars (e.g. Frogel et al. 1983). Any temperature sensitive index could in principle provide a measurement of metallicity but practical limitations such as extinction, contamination by foreground stars and calibration of the V–K$\rightarrow T_{eff}$ relationship limit their application, especially when studying high metallicity clusters in the bulge of the Galaxy.

Integrated spectroscopic IR indices have the following advantages:
i) they are intrinsically unaffected by extinction;
ii) the contamination from foreground stars is much less important than in the optical;
iii) integrated spectroscopy provide information on the global properties of the RGB which can be directly compared with the measured quantities in distant objects (ellipticals etc.).

The IR indices were selected in a study of IR spectra of cool stars (Origlia et al. 1993, hereafter OMO93) and are based on medium resolution spectra of prominent and relatively isolated features at 1.59, 1.62 and 2.29 μm whose major contributors are Si ($4s^1P^o$–$4p^1P$) and the band-heads of CO(6,3) and CO(2,0), respectively. The same absorption features were also used to study the stellar content and light to mass ratio of normal and active galaxies (Oliva et al. 1995).

This paper is structured as follows. The observational data are briefly summarized in Sect. 2. In Sect. 3 we use synthetic stellar spectra to analyze the behaviour of the selected IR indices as a function of the stellar parameters and derive a new metallicity scale. In Sect. 4 we compare our results for GGCs with the metallicities of Zinn (1985, hereafter Z85) and discuss the implications of the relatively low values of [Fe/H] we find in elliptical/spirals. In Sect. 5 we draw our conclusion.

Send offprint requests to: E.Oliva

⋆ Based on observations collected at the European Southern Observatory, La Silla, Chile

2. Observational data

The IR spectra were collected at the ESO–NTT telescope using the IRSPEC infrared spectrometer (Moorwood et al. 1991, Gredel & Weilenman 1992) equipped with a SBRC 62x58 InSb array detector. Details of observations, data reduction as well as plots of the normalized spectra which cover the central 4.4"x6.6" of each object can be found in Origlia et al. (1994) for globular clusters, and Oliva et al. (1995) for ellipticals and spirals. The last reference also describes the method used to measure the equivalent widths in spectra with velocity broadening $\sigma \geq 100$ km/s such as those found in spiral and elliptical galaxies.

The line equivalent widths listed in Table 1 were measured using the wavelength bins defined by OMO93, i.e. $W_\lambda(1.59)$, $W_\lambda(1.62)$ and $W_\lambda(2.29)$ were integrated over 1.5870–1.5910, 1.6175–1.6220 and 2.2924–2.2977 μm, respectively. The estimated accuracy is $\pm$0.5 Å for $W_\lambda(1.59)$ and $W_\lambda(1.62)$ and $\pm$1 Å for $W_\lambda(2.29)$. Note that, apart for the different units, the definition of $W_\lambda(2.29)$ is the same used by Kleinmann & Hall (1986) for their spectrophotometric CO index, numerically

$$[\mathrm{CO}]_{\mathrm{spec}} = -2.5 \log \left[1 - \frac{W_\lambda(2.29)}{53\text{Å}} \right]$$

3. A metallicity scale based on IR spectral indices

In Origlia et al. (1994) we already noticed that the IR spectral indices are well correlated with the Z85's cluster metallicities and that $W_\lambda(1.62)$ shows the steepest gradient with [Fe/H]. Here we use theoretical model stellar atmospheres and evolutionary tracks to analyze the behaviour of the IR spectral indices with stellar parameters and derive a new metallicity scale.

3.1. Synthetic stellar spectra

The variation of spectral indices with metallicity and other stellar parameters was investigated using the model stellar atmospheres of Johnson et al. (1980, hereafter J80) and Bell et al. (1990) and the spectral code described in OMO93. Briefly, this integrates the transfer equation for $\simeq$6000 lines of metals, CO, OH and produces synthetic spectra at the instrumental resolution where the equivalent widths of the features of interest are measured using the same method adopted for the observational data. More details can be found in Sect. 3.2 of OMO93.

The accuracy of the computed spectra can also depend on the quality of the adopted model stellar atmospheres. The models of J80 have been extensively used for the detailed interpretation of high resolution spectra (e.g. Lambert et al. 1984, Smith & Lambert 1985, 1990). At temperatures $\geq$4000 K the models of J80 overlap with the more recent computations of Bell et al. (1990) which we also used obtaining very similar results, the predicted equivalent widths from the two sets of models always agreed within a few percent. Any further discussion on the reliability of available model stellar atmospheres is well beyond the aims of this paper.

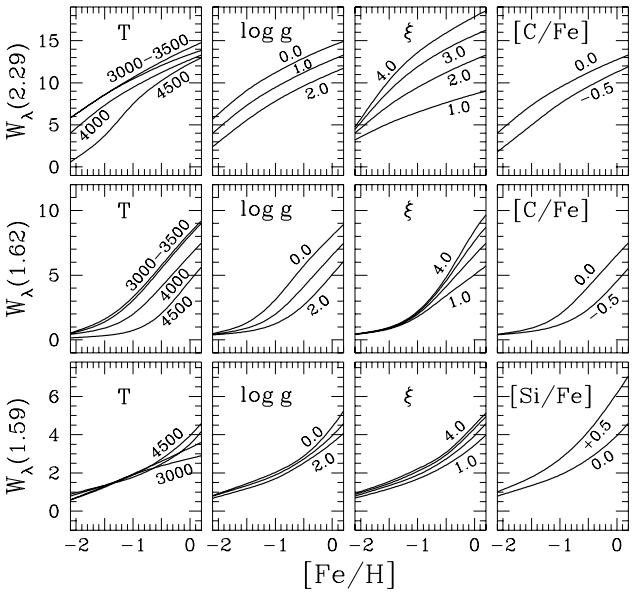

Fig. 1. Variation with metallicity of the equivalent widths (in Å) of the IR absorption features as predicted by synthetic stellar spectra. The parameters of the reference model are T_{eff}=4000 K, log g=1.0, ξ=2 km/s and solar relative abundances of metals, i.e. [C/Fe]=0.0 and [Si/Fe]=0.0. Each panel shows the effects of varying effective temperature T_{eff}, surface gravity log g, microturbulent velocity ξ and abundance anomalies [C/Fe], [Si/Fe].

A grid of about 2000 models was computed using various combinations of stellar parameters (effective temperature, surface gravity, microturbulent velocity, abundance anomalies and metallicity) covering the range

T_{eff} (K) = 3000 : 5000
log g (cm s^{-2}) = 0.0 : 2.0
ξ (km/s) = 1 : 4
[Fe/H] (dex, solar units) = –2.0 : +0.5
[C/Fe] (dex, relative to solar) = –0.5 : 0.0
[Si/Fe] (dex, relative to solar) = 0.0 : +0.5

The behaviour of the IR features can be visualized in Fig. 1 where one can notice that all stellar parameters have comparable effects on $W_\lambda(1.62)$, $W_\lambda(2.29)$ while $W_\lambda(1.59)$ is little dependent on anything but the silicon abundance. These results can be understood as follows.

The 1.59 feature is mostly due to a strong line of Si I at 1.5888 μm but is somewhat contaminated by OH Δv=2 lines at the lower temperatures and higher metallicities (cf. OMO93). At $T_{eff} \leq$5000 K silicon is mostly neutral and the Si I line lies on the damping branch of the curve of growth, its profile is dominated by the Lorentzian wings and the Γ broadening coefficient is manly provided by the natural damping ($\sim g^{-1/3}$) with a 30–50% maximum contribution by the van der Waals pressure effect ($\sim g^{1/3}$, cf. Eq. 13.24 of Gray 1976). The global gravity dependence is negligible or slightly negative. The variation with temperature and ξ is also very small except at the highest metal-

Table 1 . Observed equivalent widths and derived quantities

Object[(1)]	$[Fe/H]^{(2)}_{Lit}$ (dex)	$[Fe/H]^{(3)}_{1.62}$ (dex)	$W_\lambda(1.59)^{(4)}$ (Å)	$W_\lambda(1.62)^{(4)}$ (Å)	$W_\lambda(2.29)^{(4)}$ (Å)	$\xi^{(5)}$ (km/s)	$\Delta[C]^{(6)}$ (dex)	$\Delta[Si]^{(7)}$ (dex)
Globular Clusters								
NGC7078 (M15)	–2.15	–2.01	1.0	0.3	1.7	–	–0.01	+0.3
NGC1904	–1.68	–1.73	1.5	0.5	2.5	–	–0.41	+0.4
NGC2808	–1.37	–1.19	2.5	1.3	5.4	$\sim$1.5	+0.10	+0.9
NGC6388	–0.74	–0.64	3.2	3.0	8.6	1.5	–0.12	+0.7
NGC104 (47 Tuc)	–0.71	–0.79	3.2	2.5	8.1	1.4	–0.46	+0.6
NGC6441	–0.59	–0.84	3.0	2.3	8.1	1.5	–0.71	+0.4
NGC6624	–0.35	–1.10	3.0	1.5	7.1	$\sim$1.5	$\ll$	+0.3
NGC6553	–0.29	–0.33	3.4	4.8	12.3	2.4	–0.37	+0.2
NGC6440	–0.26	–0.36	3.5	3.9	9.1	1.4	–0.48	+0.5
Liller 1	–0.21	–0.29	3.4	4.5	10.7	1.9	–0.44	+0.3
NGC6528	+0.12	–0.23	3.7	4.6	10.4	1.7	-0.80	+0.3
Terzan 5	+0.24	–0.64	3.5	3.2	9.9	1.9	$\ll$	+0.1
Terzan 1	+0.24	+0.03	4.1	6.5	13.8	2.6	–0.60	+0.2
Ellipticals								
NGC3379	+0.09	–0.39	4.1	4.8	13.1	2.8	–1.09	+0.2
NGC4365	+0.14	–0.45	4.2	4.7	13.5	3.0	–1.28	+0.2
NGC4472	+0.08	–0.46	4.1	4.6	13.4	3.0	–1.22	+0.2
NGC7626	+0.21	–0.28	3.5	4.9	12.0	2.3	–1.07	+0.0
Spirals								
NGC779	—	–0.67	3.5	3.8	13.5	3.3	—	—
NGC995	—	–0.52	3.4	4.4	13.4	3.0	—	—
NGC1084	—	–0.61	4.0	3.5	11.0	2.3	—	—

(1) Globular clusters are ordered by increasing $[Fe/H]_{Lit}$

(2) Values of metallicity from the Literature. Globular clusters are from Z85 while for ellipticals we use Mg_2 indices by Davies et al. (1987) and the Mg_2–metallicity calibration of Casuso et al. (1996), see Sect. 4.2

(3) New estimate of [Fe/H] based on the $W_\lambda(1.62)$ index (Eqs 1,2), errors are $\pm$0.3 dex

(4) Each absorption feature is integrated on a specific wavelength range which is defined at page 540 of OMO93 (cf. Sect. 2)

(5) Microturbulent velocity derived from $W_\lambda(1.62)$ and $W_\lambda(2.29)$ (Fig. 4 and Eq. 2), errors are $\pm$0.4 km/s except for objects with $W_\lambda(1.62)<1.5$ where ξ is only poorly constrained.

(6) Δ[C] is the value of [C/Fe] necessary to reproduce the observed indices $W_\lambda(1.62)$ and $W_\lambda(2.29)$ adopting $[Fe/H]_{Lit}$, errors are typically $\pm$0.3 dex while '$\ll$' means that no solution exists (cf. Sect. 4.1 and Fig. 6)

(7) Δ[Si] is the value of [Si/Fe] necessary to obtain the observed $W_\lambda(1.59)$ adopting $[Fe/H]_{Zinn}$, errors are typically $\pm$0.5 dex

licities where the negative dependence on temperature and the more rapid increase with ξ reflects the contribution of saturated OH lines.

The behaviour of the CO–dominated features is more complex because they contain hundreds of lines some of which are saturated and therefore depend primarily on ξ, and the number of saturated lines increases at the lower temperatures and higher metallicities. The strength of the non–saturated lines is related to the column density of CO which in turn depends on the total carbon abundance (i.e. on metallicity) and surface gravity. The decrease of W_λ with increasing T_{eff} mainly reflects the variation of the fractional abundance CO/C, and this becomes negligible at temperatures $\lesssim$3500 K where most of the carbon is in the form of CO. Note that the thicker (2,0) band 'saturates' more quickly than the thinner second overtone CO(6,3). Such a different behaviour can be used to constrain the value of ξ, a parameter which cannot be easily related to theoretical predictions of stellar evolutionary models (cf. Sect. 3.4 and Fig. 4).

3.2. The relationship between metallicity and stellar parameters

The measured spectra include a large number of red giant stars which dominate the IR emission and whose average properties are primarily determined by the metallicity and, to a lesser extent, the age of the cluster. Theoretical evolutionary tracks of old stellar populations are quite well established and the weighted average of the stellar parameters

$$< T_{eff} > = \frac{\int N(L)\, L\, T_{eff}(L)\, dL}{\int N(L)\, L\, dL}$$

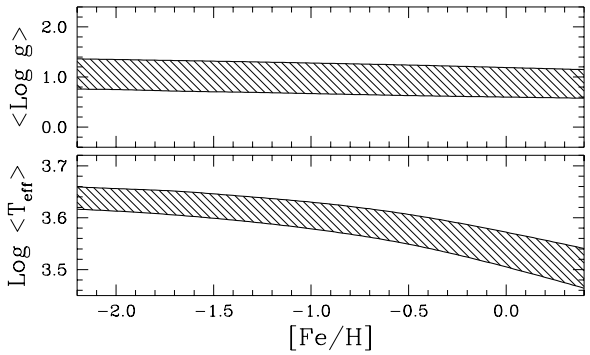

Fig. 2. Adopted average stellar parameters (effective temperature and surface gravity) as a function of cluster metallicities. The values are based on theoretical evolutionary tracks and their 'uncertainties' indicated by the shaded areas includes a broad range of stellar luminosities and differences between different models (cf. Sect. 3.2 for details).

$$< \log g > \; = \; \frac{\int N(L)\, L \log g(L)\, dL}{\int N(L)\, L\, dL}$$

can be easily computed from published tables. The results are virtually independent of the assumed initial mass function because of the very rapid increase of luminosity on the RGB. Noticeably, the relationship between the IR luminosity L at 1.6 or 2.2 μm and the bolometric luminosity from the models is much less uncertain than the $M_{bol} \rightarrow M_V$ conversion which suffers by large errors in the cooler and most metallic stars.

The observed IR emission is therefore dominated by relatively few red giants with luminosity within a factor of ≈4 of L(RGB–tip) and, to a first approximation, the average temperatures and gravities are those of the stars with $M_{bol} \simeq -3$ or half of the RGB maximum luminosity. The main uncertainties on the computed values are related to the treatment of convection in evolutionary models (e.g. Straniero & Chieffi 1991 and references therein) and statistical fluctuations in the observed field of view which may not properly sample the most luminous RGB stars (cf. end of Sect. 3.4).

The adopted relationship between $< T_{eff} >$, $< \log g >$ and metallicity is plotted in Fig. 2 and is based on the evolutionary tracks of Straniero & Chieffi (1991) and Maeder & Meynet (1989). The scatter takes into account age variations between 10 and 20 Gyr and luminosity fluctuations of 2 magnitudes. The 'observed' RGB temperatures (derived from V–K colours, Frogel et al. 1983) lie within the spread of $< T_{eff} >$ in Fig. 2.

Note that the CO–dominated features are little sensitive to T_{eff} when the stellar temperature is lower than 3500 K (cf. Fig. 1). Consequently, the predicted values of $W_\lambda(1.62)$ and $W_\lambda(2.29)$ (Fig. 3a) are virtually unaffected by the choice of the lower limit on $< T_{eff} >$ of Fig. 2.

3.3. The metallicity dependence of IR spectral indices

The variation of equivalent widths with metallicities is plotted in Figs. 3a, 3b. The dashed areas correspond to the spread of the stellar parameters vs. metallicity relationships of Fig. 2, and

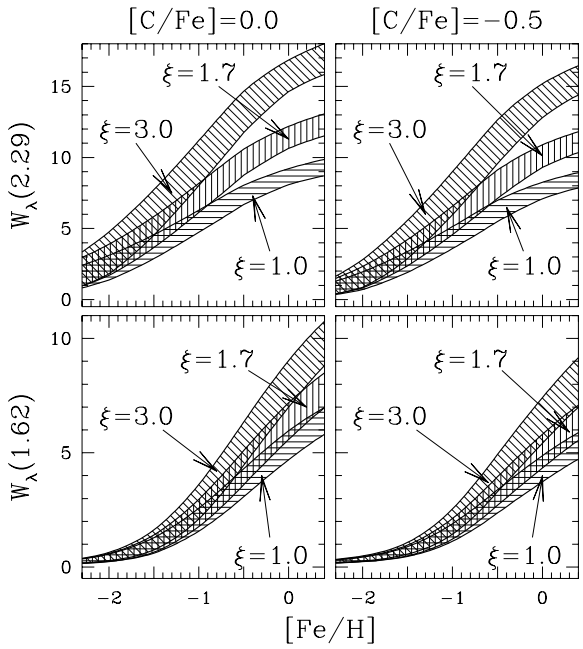

Fig. 3a. Predicted variation of the CO–dominated indices as a function of cluster metallicity for solar [C/Fe] (left) and a Carbon depletion of –0.5 dex (right hand panels). At each metallicity a large grid of models with different stellar parameters and T_{eff}, $\log g$ within the range of Fig. 2 were computed. The range of equivalent widths obtained is indicated by the shaded areas. Note the strong effect of the microturbulent velocity ξ on the CO(2,0) band at 2.29 μm, this index can be used to extimate ξ (cf. Fig. 4). The behaviour of $W_\lambda(1.62)$ can be accurately reproduced by the interpolation formula given in Eqs. 1a, 1b.

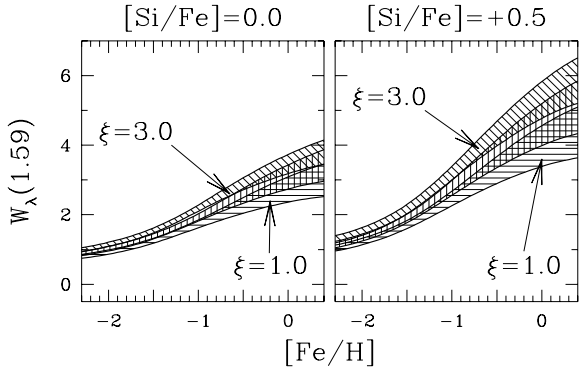

Fig. 3b. Same as Fig. 3a for the 1.59 μm features, note that $W_\lambda(1.59)$ grows quite slowly with [Fe/H].

the curves for different microturbulent velocities are displayed separately to visualize the effect of ξ on the various features. Evident is the strong variation of $W_\lambda(2.29)$ with ξ while $W_\lambda(1.62)$ increases rapidly with [Fe/H] and is much less sensitive to the value of the microturbulent velocity. The variation of $W_\lambda(1.62)$ with [Fe/H] is accurately reproduced by the handy relationships

$$\text{[Fe/H]} = 1.3 \log \{W_\lambda(1.62)\} - 0.47\text{[C/Fe]} - 0.05\xi - 1.4$$

$$\pm 0.15 \qquad\qquad W_\lambda(1.62) < 2\text{Å} \qquad (1a)$$

$$[\mathrm{Fe/H}] = \frac{0.33 - 0.1[\mathrm{C/Fe}]}{\sqrt{\xi}} \{W_\lambda(1.62) - 2.0\} - 0.47[\mathrm{C/Fe}] -$$

$$-0.05\xi - 1.00 \pm 0.15 \qquad W_\lambda(1.62) > 2\text{Å} \qquad (1b)$$

where the spread of $\pm$0.15 corresponds to the width of the dashed areas of Fig. 3a. Noticeably, the value of $W_\lambda(1.62)$ is relatively little sensitive to the carbon depletion and an uncertainty of $\pm$0.3 dex in [C/Fe] only produces an error of about $\pm$0.15 dex in [Fe/H]. The reason for this behaviour is because the growth of $W_\lambda(1.62)$ with metallicity tracks the decrease of T_{eff} and $\log g$ (cf. Fig. 1 and Fig. 2), and is only partly related to increase of carbon abundance. Roughly speaking, the factor of $\sim$3 growth of $W_\lambda(1.62)$ between [Fe/H]=–1.0 and 0.0 is equally distributed between the effects of decreasing temperature and gravity, and increasing carbon abundance.

The strength of the 1.59 μm feature is much less sensitive to [Fe/H] and the metallicities derived from $W_\lambda(1.59)$ are therefore quite uncertain, the spread of the dashed areas in Fig. 3b corresponds to $\pm$0.5dex in [Fe/H]. Besides, $W_\lambda(1.59)$ is unable to distinguish between variations of [Fe/H] and [Si/Fe] because this index is virtually independent of stellar parameters others than the silicon abundance (cf. Sect. 3.1 and Fig. 1). Consequently, any uncertainty in [Si/Fe] directly translates into an error in [Fe/H]. The value of $W_\lambda(1.59)$ does not therefore provide a reliable estimate of metallicity though it may give some indication of the Si relative abundance in old stellar clusters where the α elements, like Si itself, should be significantly enhanced (Kraft 1994 and reference therein). This issue is analyzed in Sect. 4.3

3.4. Constraints on microturbulent velocities

The microturbulent velocity ξ strongly influences the strength of saturated molecular lines but cannot be easily connected to photospheric temperature, surface gravity or other physical conditions of a given star. Observationally, ξ appears to be correlated with the stellar luminosity and spectral studies at high resolution of field red giants indicate $\xi \sim 2$ km/s with an increase of about 0.8 km/s when the stellar temperature decreases from 4300 K to 3100 K (McWilliam & Lambert 1984, Smith & Lambert 1985).

Although theoretical arguments constraining ξ are missing, its value can be estimated by comparing the strength of the thick CO(2,0) with the thinner CO(6,3) band–heads. The different behaviour of the CO–dominated indices with ξ is clearly visible in Fig. 3a but can be more conveniently visualized and quantified using a plot of $W_\lambda(1.62)$ versus the ratio $W_\lambda(1.62)/W_\lambda(2.29)$. In such a diagram (Fig. 4) cooler and more metallic objects lie at the top right, and those with larger microturbulent velocities lie on the left because they have stronger CO(2,0). The theoretical curves plotted in Fig. 4 are based on the grid of synthetic spectra described above using the relationships between metallicity and T_{eff},$\log g$ of Fig. 2. Noticeably, the shaded areas in Fig. 4 are quite narrow, i.e. the spread of the theoretical curves at ξ=constant is small because changing T_{eff}, $\log g$ or [C/Fe] for a given metallicity mainly moves the points along, and not perpendicularly to the curves.

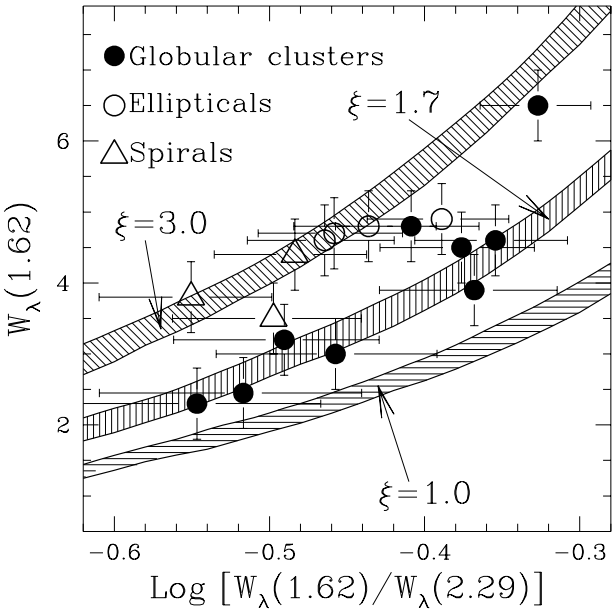

Fig. 4. Observed and predicted behaviours of the CO–dominated indices bands. The data are plotted in the spectroscopic equivalent of a colour–magnitude diagram where the 'magnitude' is $W_\lambda(1.62)$ while the 'colour' is the logarithm of the ratio of the equivalent widths of the 1.62 and 2.29 μm features. The shaded areas show the range covered by models with constant microturbulent velocity ξ, the theoretical results can be accurately reproduced by the fitting relationship $y = -0.6 - \xi - 2\xi^{0.8}/(x - 0.07\sqrt{\xi})$ where $y = W_\lambda(1.62)$ and $x = \log[W_\lambda(1.62)/W_\lambda(2.29)]$.

The value of ξ in a given object can be estimated graphically or using the fitting formula given in the caption of Fig. 4 which yields

$$\xi = \frac{-xy - 0.6x}{x + 2\xi^{-0.2} - 0.07\xi^{0.5} - (0.042 + 0.07y)\xi^{-0.5}} \qquad (2)$$

where y=$W_\lambda(1.62)$ and x=$\log[W_\lambda(1.62)/W_\lambda(2.29)]$, this equation can be resolved iteratively.

The derived values of ξ are listed in Table 1 and vary from $\simeq$1.5 in the least metallic clusters to about 3 km/s in the coolest objects, in good agreement with the detailed studies of field stars quoted above. Variations of ξ between globular clusters with similar $W_\lambda(1.62)$ or metallicity are only marginally significant (cf. the error bars in Fig. 4), but galaxies have systematically larger microturbulent velocities, and this could be explained as follows. Under the reasonable assumption that microturbulent velocities increase with stellar luminosity along the RGB, the stars with larger ξ are those closer to the RGB–tip. These cool and very luminous objects contribute to a large fraction of the 1.6 μm emission but are very rare: numerical simulations indicate that the central $\oslash$6" of a massive globular cluster like 47Tuc should on average contain less than 1 star with luminosity $L > 0.5L$(RGB–tip). It is therefore likely that this stellar population was not properly sampled in our instrumental aperture (4.4"x6.6"), i.e. in GGCs we probably missed some of the most luminous (and high–ξ) red giants. In external galaxies the

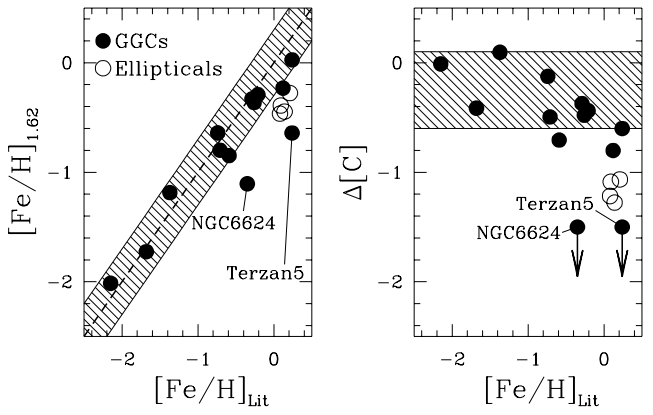

Fig. 5. Left panel: comparison between the metallicities derived from $W_\lambda(1.62)$ and values of [Fe/H] from the literature: Z85 for globular clusters and the Casuso et al. (1996) calibration of the Mg_2 index for ellipticals. The dashed area is $\pm$0.3 dex and corresponds to the expected uncertaininty of the $[Fe/H]_{1.62}$ calibration. Note the large discrepancies for elliptical galaxies and the marked globular clusters,
Right hand panel: Δ[C] is the value of [C/Fe] to match the values of $[Fe/H]_{1.62}$ and $[Fe/H]_{Lit}$. Points falling within the dashed areas are compatible within the errors with an average Carbon depletion of about –0.3 dex. The arrows on NGC6624 and Terzan 5 indicate that no solution exists for these objects: below [C/Fe]=–1.5 the $W_\lambda(1.62)$ index is dominated by OH and Ca lines and no longer depends on the Carbon relative abundance (cf. Fig. 6).

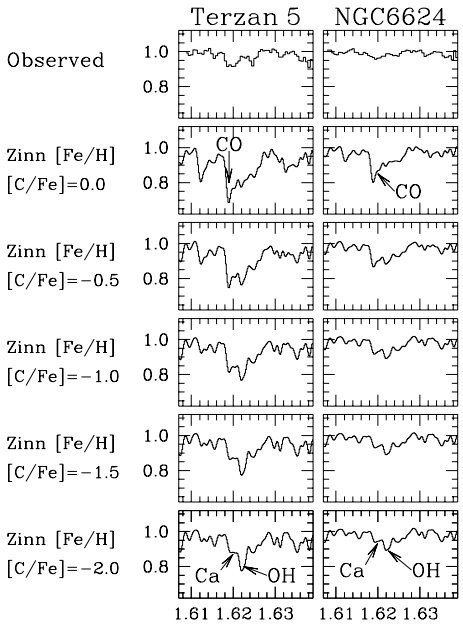

Fig. 6. Effects of varying the Carbon relative abundance [C/Fe] on the spectrum around 1.62 μm. The top figures are the observed data while the other panels show the results of synthetic spectra computed for different [C/Fe] adopting Zinn's metallicities (Z85), stellar parameters from Fig. 2 and ξ from Table 1. Spectra with undepleted Carbon are dominated by the bandhead of CO(6,3) (indicated by the arrow) which becomes much less evident at [C/Fe]$\simeq$–1.0 and virtually disappears at larger Carbon depletions where the spectrum is dominated by OH and Ca lines and the $W_\lambda(1.62)$ index does not any longer depend on [C/Fe]. Our spectra indicate therefore that the two clusters are much less metallic than presently believed.

spectrometer slit samples $> 10^4$ more stars than in a GGC, statistical fluctuations are therefore unimportant and the observed spectrum is in all cases dominated by the most luminous (and higher–ξ) giants close to the RGB–tip.

4. Comparison with other metallicity estimates

4.1. Globular clusters

The metallicities derived from the $W_\lambda(1.62)$ index adopting a 'standard' [C/Fe] depletion of –0.3 dex (Lambert and Ries 1977, 1981, Kraft 1994) and the values of ξ derived above are listed in Table 1 together with the Z85's metallicities (Z85) for GGCs. A comparison between the two sets of data is displayed in Fig. 5 (left panel, filled circles). Also plotted in the right–hand panel of Fig. 5 are the carbon depletions (ΔC) necessary to obtain the observed $W_\lambda(1.62)$ adopting the cluster metallicities of Z85.

Table 1 and Fig. 5 show that the metallicities derived from $W_\lambda(1.62)$ are equal within the errors to the Z85's values for most GGCs. The most remarkable exceptions are NGC6624 and Terzan 5 for which we find values of [Fe/H] lower by 0.8 and 0.9 dex, respectively. This discrepancy cannot be ascribed to large C depletion, this is evident in Fig. 6 which compares observed and synthetic spectra computed assuming Z85's metallicities and different values of [C/Fe]. Varying the C depletion has a significant effect on $W_\lambda(1.62)$ only for [C/Fe]$\gtrsim$–1.0, but for a larger carbon depletion the CO(6,3) band–head virtually disappears and the spectrum is dominated by OH features which are not visible in the data.

Apart for the the above discrepancies, the right hand panel of Fig. 5 gives also a marginal evidence that the carbon depletion becomes more significant in higher metallicity clusters. This may either indicate that [C/Fe] is a function of [Fe/H] or that available [Fe/H] estimates are systematically overestimated in objects with quasi solar metallicities. We tend to favour the second hypothesis because carbon depletions larger than 0.5 dex would strongly modify the 1.62 μm line profile (cf. Fig. 6) and we do not observe any such distortion in our spectra.

The above comparison indicates therefore that metallicities derived from $W_\lambda(1.62)$ should be accurate within a generous error of $\pm$0.3 dex which includes the spread of theoretical predictions (the shaded areas of Fig. 3a), a $\pm$0.3 dex uncertainty on [C/Fe] (which translates into a $\pm$0.15 dex in [Fe/H], cf. Sect. 3.2), a $\pm$0.5 km/s uncertainty in the microturbolence velocity and observational errors. Also, our IR spectra provide strong evidence that NGC6624 and Terzan 5 are much less metallic than presently believed.

4.2. Elliptical and spiral galaxies

Few estimates of metallicities in elliptical galaxies exist in the literature, and these are mostly based on measurements of the strong Mg_2 index. The most recent Mg_2 vs. metallicity calibra-

tion is that of Casuso et al. (1996) who also review previous works on the subject. The values of [Fe/H] listed in 2nd column of Table 1 are based on the Mg_2 measurements of Davies et al. (1987) using the 17 Gyr models of the above reference. Noticeably, these are *lower limits* for Mg_2 metallicities because using different calibrations and/or younger ages requires a larger [Fe/H] to match the observed Mg_2 strength (cf. Figs. 1, 2 of Casuso et al. 1996).

The metallicities derived here are significantly lower than solar (–0.5 to –0.3) and systematically smaller by about 0.55 dex than those inferred from Mg_2. As the latter index is primarily a measurement of the magnesium abundance and any variation of [Mg/Fe] translates into a similar variation of [Fe/H], the above difference could therefore indicate a magnesium enhancement [Mg/Fe]$\simeq$0.5, as already suggested by other authors (Buzzoni et al. 1992, 1994, Carollo & Danziger 1994a,b, McWilliam & Rich 1994).

The metallicities derived for the three spirals in our sample are only slightly lower ($\sim$0.2 dex) than those of ellipticals. No other measurements of metallicity are available for these little studied objects.

4.3. silicon abundance

The strength of the 1.59 μm feature is primarily sensitive to the total silicon abundance [Si/H] but varies quite slowly with this parameter (cf. end of Sect. 3.3). It could be however useful to obtain an estimate of the Si relative abundance [Si/Fe] which, alike other α elements, should be enhanced by 0.3–0.5 dex (Kraft 1994). Table 1 (last column) and Fig. 7 (left panel) show the values of [Si/Fe] obtained adopting Z85's metallicities for GGCs and Mg_2 metallicities for ellipticals. Apart from the large scatter of the points, the most significant result is that elliptical galaxies and the most metallic clusters have silicon enhancements close to zero and lie well below lower metallicity objects in the left diagram of Fig. 7. This trend disappears when the value of [Fe/H] is derived from $W_\lambda(1.62)$, and [Si/Fe] becomes $\sim$0.5 for most objects when the $[Fe/H]_{1.62}$ metallicity scale is adopted (cf. the right hand panel of Fig. 7).

The above results indicate that silicon is enhanced by about 0.5 dex in both globular clusters and ellipticals, the Si overabundance is therefore similar to that of magnesium (Sect. 4.2). Consequently, objects with [Fe/H] derived from the Mg_2 index tend to show solar [Si/Fe] because their metallicity is overestimated and this effect is particularly evident in elliptical galaxies and highly metallic GGCs. In other words, indices based on lines of Mg, Si and other α elements tend to overestimate [Fe/H] and may lead to confusing results on the relative abundances (enhancements) of these species.

5. Conclusions

We analyzed and modelled integrated infrared spectra of Galactic globular clusters and elliptical/spiral galaxies centered around prominent and relatively isolated stellar absorption features at 1.59, 1.62 and 2.29 μm whose major contributors are a strong SiI line and the band-heads of CO(6,3) and CO(2,0), respectively. Synthetic spectra from model stellar atmospheres coupled with theoretical evolutionary tracks show that $W_\lambda(1.62)$ provides measurements of metallicity accurate to within $\pm$0.3 dex and which can be readily computed using handy interpolation formulae (Eqs. 1a, 1b) where the photospheric microturbulent velocity ξ can be set to a fiducial value of 1.7 km/s or estimated from measurements of $W_\lambda(2.29)$ (Fig. 4 and Eq. 2). Anomalies of the carbon abundance, [C/Fe], have relatively little influence on the derived metallicities: an error of 0.3 dex in [C/Fe] translates into a $\pm$0.15 uncertainty in [Fe/H]. The physical reason for this result is that the growth of $W_\lambda(1.62)$ with metallicity is primarily driven by the decrease of T_{eff} and $\log g$ with [Fe/H], while is only partly related to the increase of the total carbon abundance. Moreover, carbon depletions much lower than –0.5 dex can be easily recognized (and in our case excluded) from the shape of the spectrum around 1.62 μm which should become dominated by OH lines (Fig. 6).

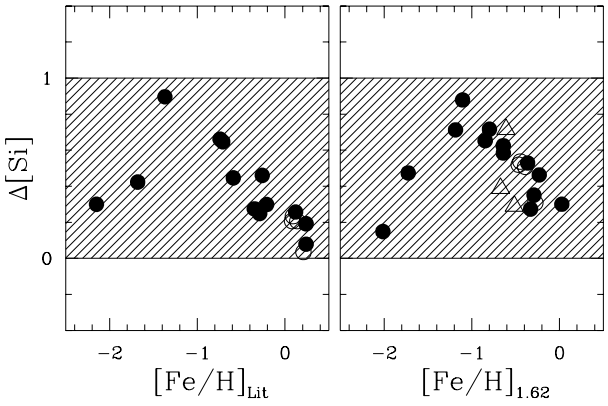

Fig. 7. Δ[Si] is the value of [Si/Fe] necessary to obtain the observed strength of the index $W_\lambda(1.59)$ adopting values of [Fe/H] from the literature (left panel) and the metallicities derived from $W_\lambda(1.62)$ (right hand panel), typical errors are $\pm$0.5 dex and the results are compatible with Δ[Si]=0.5$\pm$0.5 (the shaded areas), see Sect. 4.3 for details.

Using a 'standard' C–depletion of [C/Fe]=–0.3 we accurately reproduce Z85's metallicities for most globular clusters with however two remarkable exceptions, namely NGC6624 and Terzan 5, for which we find metallicities lower by 0.8 and 0.9 dex, respectively, and these discrepancies cannot be explained by anomalous carbon abundances (Fig. 6). In ellipticals we find [Fe/H] values between –0.5 and –0.3 and $\sim$0.5 dex lower than current estimates based on Mg_2 indices. This discrepancy cannot be easily ascribed to large carbon depletions but indicates that Mg and other α elements should be enhanced by $\sim$0.5 dex. This conclusion is further supported by our measurements of the strong line at 1.59 μm whose large equivalent widths require [Si/Fe]$\sim$0.5 dex in most objects.

The 'classical' index based on the strength of the CO first overtone band at $\lambda \geq 2.29$ μm is a poor indicator of metallicity because it primarily depends on the atmospheric microturbulent velocity ξ which is only accidentally related with [Fe/H]. The CO(2,0) index is however useful in combination with $W_\lambda(1.62)$

to estimate ξ (Fig. 4 and Eq. 2) which was found to vary between 1.5 and 3 km/s (Table 1), in agreement with previous results.

References

Bell R.A., Briley M.M., Smith G.H., 1990, AJ 100, 187
Buzzoni, A., Mantegazza L., Gariboldi G., 1992, AJ 103, 513
Buzzoni, A., Mantegazza L., Gariboldi G., 1994, AJ 107, 513
Carollo M.C., Danziger I.J., 1994a, MNRAS 270, 523
Carollo M.C., Danziger I.J., 1994b, MNRAS 270, 743
Casuso E., Vazdekis A., Peletier R.F., Beckman J.E., 1996, ApJ 458, 533
Davies R.L., Burstein D., Dressler A., Faber S.M., Lynden–Bell D., Terlevich R.J., Wegner G., 1987, ApJS 64, 581
Frogel J.A., Cohen, J.G., Persson S.E.: 1983, ApJ 275, 773
Gray D.F, 1976, *The Observation and Analysis of Stellar Photospheres*, Wiley-Interscience Pub., New York
Gredel R., Weilenman U., 1992, The Messenger 70, 62
Johnson H.R., Bernat A.P., Krupp B.M., 1980, ApJS 42, 501 (J80)
Kleinmann S.G., Hall D.N.B., 1986, ApJS 62, 501
Kraft R.P., 1994, PASP 106, 553
Lambert D.L., Ries L.M., 1977, ApJ 217, 508
Lambert D.L., Ries L.M., 1981, ApJ 248, 228
Lambert D.L., Brown J.A., Hinkle K.H., Johnson H.R., 1984, ApJ 284, 223
Maeder A., Meynet G., 1989, A&A 210, 155
McWilliam A., Lambert D.L., 1984, PASP 96, 882
McWilliam A., Rich R.M., 1994, ApJS 91, 749
Moorwood A.F.M., Moneti A., Gredel R., 1991, The Messenger 63, 77
Oliva E., Origlia L., Kotilainen J.K., Moorwood A.F.M., 1995, A&A 311, 55
Origlia L., Moorwood A.F.M., Oliva E., 1993, A&A 280, 536 (OMO93)
Origlia L., Moorwood A.F.M., Oliva E., 1994, The Messenger 75, 21
Smith V.V., Lambert D.L., 1985, ApJ 294, 326
Smith V.V., Lambert D.L., 1990, ApJS 72, 387
Straniero O., Chieffi A., 1991, ApJS 76, 525
Zinn R.J., 1985, ApJ 293, 324 (Z85)

This article was processed by the author using Springer-Verlag LaTeX A&A style file *L-AA* version 3.